Semiconductor Physics, Quantum Electronics & Optoelectronics, 2026. V. 29, No 1. P. 028-035.

Semiconductor physics

Structure–property relationships in $Ag_{6+x}(P_{1-x}Si_x)S_5I$ argyrodite-type solid solutions

A.I. Pogodin[1*], M.J. Filep[2], I.O. Shender[1], T.O. Malakhovska[1], O.P. Kokhan[1], V. Izai[3]

[1]*Uzhhorod National University, 46, Pidhirna str., 88000 Uzhhorod, Ukraine*
[2]*Ferenc Rakoczi II Transcarpathian Hungarian University, 6, Kossuth Sq., 90200 Beregovo, Ukraine*
[3]*Comenius University, Mlynska dolina, Bratislava 84248, Slovakia*
[*]*Corresponding author e-mail: artempogodin88@gmail.com*

Abstract. In this work, single crystals of solid solutions $Ag_{6.25}P_{0.75}Si_{0.25}S_5I$ and $Ag_{6.75}P_{0.25}Si_{0.75}S_5I$ were obtained and studied. The synthesis was carried out using a one-temperature method, and the single crystals were grown by directional crystallization from a melt. Single crystals with a diameter close to 1.2 cm and a length of 3–4 cm were grown. The crystal structure was studied using XRD with the Rietveld analysis. It was found that solid solutions crystallize in the space group F-43m, $Z = 4$, with parameters $a = 10.549$ Å ($Ag_{6.25}P_{0.75}Si_{0.25}S_5I$) and $a = 10.604$ Å ($Ag_{6.75}P_{0.25}Si_{0.75}S_5I$). Electrical properties were studied using impedance spectroscopy within a wide temperature and frequency range. It was shown that the electrical conductivity is predominantly ionic, with the ionic component exceeding the electronic component by 10^4 times. It was found that with increasing the silicon content, ionic electrical conductivity increases (up to 10^{-2} S/cm), and its activation energy decreases. The obtained results are explained by the peculiarities of the crystal structure, namely by changes in the position, coordination, and dimensional arrangement of mobile Ag^+ ions.

Keywords: argyrodite, single crystal, ionic conductivity, solid solutions.

https://doi.org/10.15407/spqeo29.01.028
PACS 61.50.-f, 66.30.Dn, 81.10.Fq

Manuscript received 22.11.25; revised version received 09.02.26; accepted for publication 18.03.26; published online 25.03.26.

1. Introduction

Global trends in energy development are focused on implementing the energy-saving and resource-efficient approaches based on improved energy storage technologies. Electrochemical storage systems play an important role in this context, with lithium-ion batteries currently dominating the market [1]. Their popularity is due to a combination of high specific energy, fast charging, low weight, and compactness [2]. The further development of lithium-ion systems is associated to the creation of all-solid-state batteries (ASSB), in which liquid electrolytes are replaced by solid ion conductors. This approach significantly improves safety, increases energy density, and extends battery life by eliminating the key drawbacks of modern electrochemical power sources [3, 4]. At the same time, the efficiency of ASSBs is directly determined by the properties of solid ion conductors, which should combine high ionic and minimal electronic conductivity, stability in chemical and electrochemical environments, and mechanical reliability within a wide range of operating conditions [5, 6].

Solid electrolytes belong to several classes. Oxide systems, in particular perovskites and garnet-like structures, are characterized by high chemical stability but limited ionic conductivity at room temperature [7, 8]. Polymer electrolytes are lightweight and flexible but inferior in terms of transport characteristics [9, 10]. Sulfide solid electrolytes are considered the most promising, as their ionic conductivity can reach the level of liquid electrolytes, although stability remains insufficient for lithium-containing compounds [11, 12].

Among sulfide ionic conductors, materials with mobile Ag^+ ions are of considerable interest due to their low effective mass, high polarizability, and ability to migrate rapidly in the crystal lattice [13]. Simple silver sulfide exhibits high ionic conductivity, but its practical use is limited by phase transformations [14, 15]. More promising are multicomponent compounds – argyrodites with a complex crystal structure, in which a rigid anionic framework is combined with partially occupied silver positions [16, 17]. For solid conductors, the most suitable is statistical distribution of Ag^+ ions, realized in F-43m-type space group (SG) structures, that ensures effective ion

diffusion and thus high ionic conductivity: $8.13\cdot10^{-3}$ S/cm (Ag_7SiS_5I [18]), $7.98\cdot10^{-3}$ S/cm (Ag_7GeS_5I [18]), $1.79\cdot10^{-3}$ S/cm (Ag_6PS_5I [19]). Additionally, the similar structure of argyrodites contributes to forming a solid solution by iso- and heterovalent substitutions, effectively controlling ionic conductivity and converting low-conductivity phases into a superionic state [18, 20].

This work aims to synthesize and experimentally study the electrical properties of $Ag_{6.25}P_{0.75}Si_{0.25}S_5I$ and $Ag_{6.75}P_{0.25}Si_{0.75}S_5I$ single crystals with an argyrodite structure to ascertain the relationship between their chemical composition, crystal structure, and functional characteristics.

2. Experimental

The synthesis of $Ag_{6.25}P_{0.75}Si_{0.25}S_5I$ and $Ag_{6.75}P_{0.25}Si_{0.75}S_5I$ solid solutions was performed using a one-temperature method in quartz ampoules evacuated to 0.13 Pa from pre-synthesized Ag_6PS_5I and Ag_7SiS_5I taken in the corresponding stoichiometric ratios. The latter were synthesized according to the procedure described in detail in Refs. [18, 19]. The ampules containing the initial materials were heated to 950 °C at a rate of 100 °C/h and held at this temperature in the melt for 72 h, which ensured the completion of the component interaction. The temperature was then lowered to room temperature at a rate of 50 °C/hour. As a result, bulk polycrystalline alloys $Ag_{6.25}P_{0.75}Si_{0.25}S_5I$ and $Ag_{6.75}P_{0.25}Si_{0.75}S_5I$ were obtained, each weighing 20 g. The obtained alloys were transferred to quartz ampules with conical bottoms for the crystal growth *via* directional crystallization from the melt. The detailed technological regimes of growing the $Ag_{6.25}P_{0.75}Si_{0.25}S_5I$ and $Ag_{6.75}P_{0.25}Si_{0.75}S_5I$ single crystals are described in Ref. [21]. As a result, dark gray single crystals with a metallic luster, 1.2 cm in diameter and 3–4 cm in length, were obtained.

The grown single crystals were studied using X-ray diffraction (XRD) and impedance spectroscopy (EIS) methods. For XRD analysis, the AXRD Benchtop (Proto Manufacturing Limited) equipped with a DECTRIS MYTHEN2 R 1D detector, Bragg–Brentano θ/2θ imaging geometry, Ni filtered CuK_α radiation, 10–120° 2θ angle scanning range with a dynamic region of interest, and 1 s exposure was used. The EIS method was realized using the high-precision LCR meter AT 2818 with a frequency range of $1\cdot10^1$ to $3\cdot10^5$ Hz, temperature range of 20 to 110 °C, and AC amplitude of 10 mV. The measurements were performed using gold contacts deposited by chemical deposition from solutions [22].

The structural parameters were calculated using the Rietveld method [23, 24] in the EXPO 2014 program [25, 26]. The visualization of crystal structures and the determination of the parameters of structure-forming polyhedra were performed in the VESTA 3.5.7 program [27]. An analysis of frequency dependences of the total electrical conductivity was performed using the ZView 3.5 program. The analysis considered the cell inductance equal to $2\cdot10^{-8}$ H.

3. Results and discussion

3.1. Crystal structure

Let us consider the crystal structures of $Ag_{6+x}(P_{1-x}Si_x)S_5I$ single crystals. It should be noted that the crystal structure of $Ag_{6.5}P_{0.5}Si_{0.5}S_5I$ single crystals is discussed in detail in Ref. [21]. Based on this, the results of full-profile analysis using the Rietveld method (Fig. 1) indicate that the solid solutions $Ag_{6.25}P_{0.75}Si_{0.25}S_5I$ and $Ag_{6.75}P_{0.25}Si_{0.75}S_5I$ crystallize in the argyrodite-type structure with SG F-43m, Z = 4, a = 10.549 Å ($Ag_{6.25}P_{0.75}Si_{0.25}S_5I$), a = 10.604 Å ($Ag_{6.75}P_{0.25}Si_{0.75}S_5I$). The reliability of the ascertained structural parameters is confirmed by low R_{wp} values: 2.207% for $Ag_{6.25}P_{0.75}Si_{0.25}S_5I$, 2.612% for $Ag_{6.75}P_{0.25}Si_{0.75}S_5I$, and concurrence of the calculated and experimental curves in Fig. 1.

It has been ascertained that heterovalent cationic $P^{+5} \rightarrow Si^{+4}$ substitution, which causes the formation of $Ag_{6+x}(P_{1-x}Si_x)S_5I$ solid solutions, occurs in one position (4b), leading to the formation of common P(Si) positions in the crystal structure (Fig. 2). These common P(Si) positions are coordinated by four sulfur atoms S1 in position 16e, forming corresponding $[P(Si)S_4]$ tetrahedra (Fig. 2), which are the basis of a rigid anionic sublattice. It should be noted that these tetrahedra are characterized by the absence of distortion.

In the structures of $Ag_{6.25}P_{0.75}Si_{0.25}S_5I$ and $Ag_{6.75}P_{0.25}Si_{0.75}S_5I$ crystals, there are two symmetrically independent positions of silver Ag1 (24g) and Ag2 (48h) in which the site occupancy factor (SOF) is less than 1, indicating their statistical placement in symmetrically equivalent positions. The Ag1 (24g) position is in a triangular coordination S1S2S2, while Ag2 (48h) is tetrahedrally coordinated by three sulfur atoms in positions S1S2S1 and an iodine atom I1 in position 4a (Fig. 2). It should be noted that due to the statistical occupancy of positions, these silver atoms form a cationic sublattice, which is disordered.

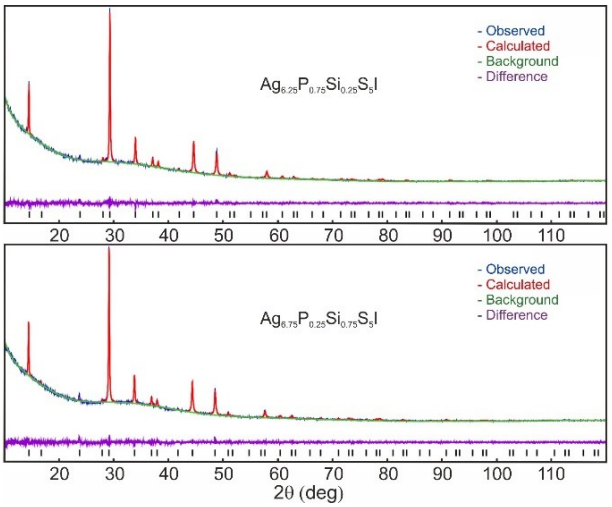

Fig. 1. Calculated and experimental powder patterns for $Ag_{6+x}(P_{1-x}Si_x)S_5I$ solid solutions.

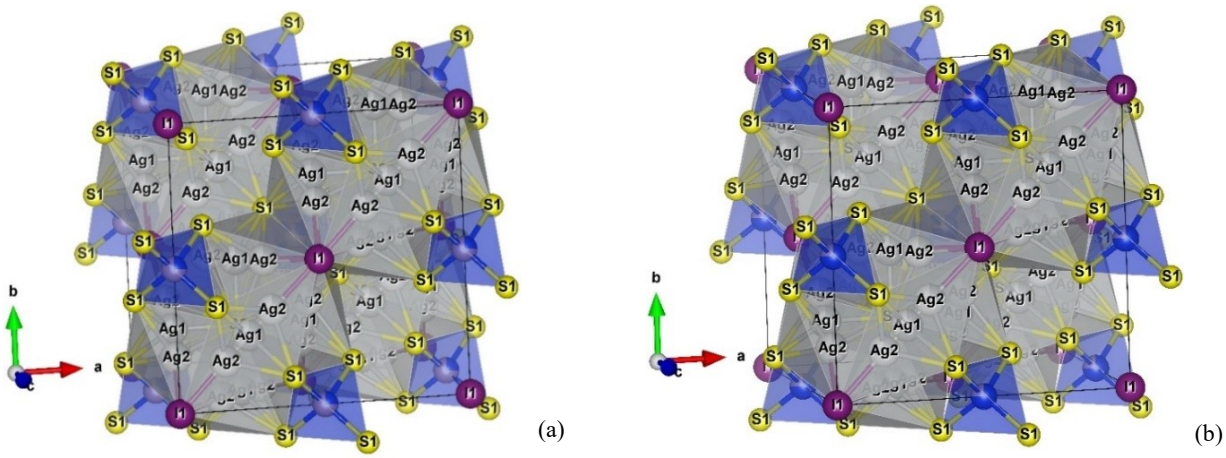

Fig. 2. Unit cells and structure-forming polyhedra in the crystal structures of $Ag_{6.25}P_{0.75}Si_{0.25}S_5I$ (a) and $Ag_{6.75}P_{0.25}Si_{0.75}S_5I$ (b) single crystals.

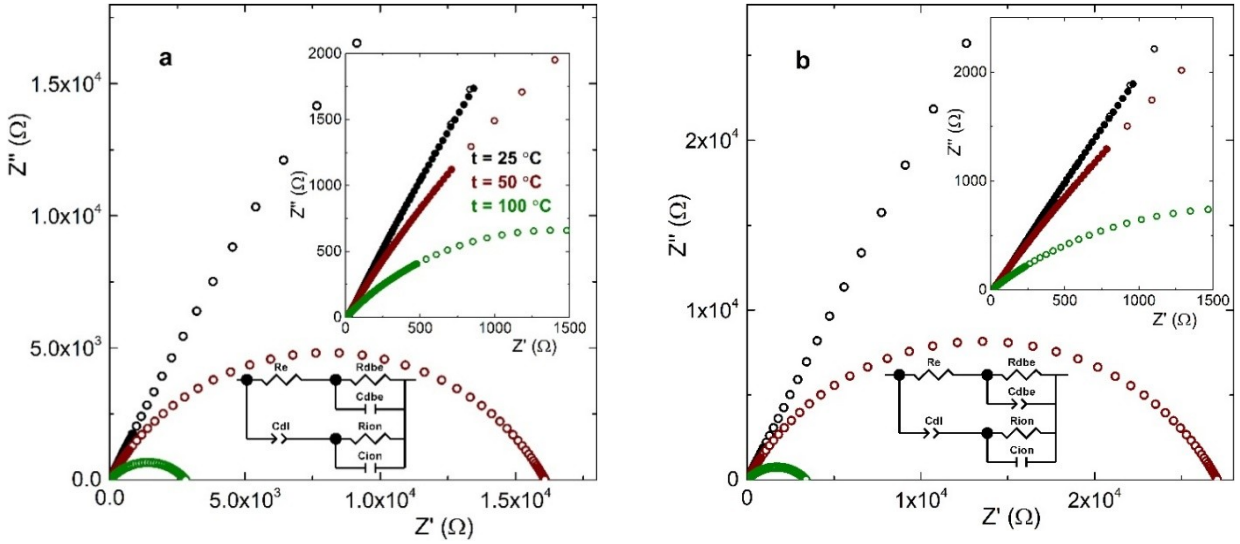

Fig. 3. Nyquist plots and EEC for $Ag_{6.25}P_{0.75}Si_{0.25}S_5I$ (a) and $Ag_{6.75}P_{0.25}Si_{0.75}S_5I$ (b) crystals at various temperatures (filled rings designate experimental data, unfilled rings – fitted by EEC).

3.2. Electrical conductivity

The frequency dependences of the total electrical conductivity of $Ag_{6.25}P_{0.75}Si_{0.25}S_5I$ and $Ag_{6.75}P_{0.25}Si_{0.75}S_5I$ crystals are similar and typical for materials with ionic electrical conductivity in the solid state. That is, with increasing frequency, the total electrical conductivity increases sharply. A standard approach [28] based on the analysis of electro-chemical equivalent circuits (EEC) of Nyquist plots (Fig. 3) was used to determine the parameters of ion transport and the electronic component of electrical conductivity.

In the Nyquist plots (Fig. 3) within 30…110 °C ($Ag_{6.25}P_{0.75}Si_{0.25}S_5I$) and 40…110 °C ($Ag_{6.75}P_{0.25}Si_{0.75}S_5I$), arc-shaped sections (low-frequency region) with deformation within the high-frequency region are observed, while at lower temperatures the low-frequency sections are linear. This is explained by the low values of electronic conductivity, which cannot be determined below these temperatures. Therefore, at temperatures below 30 °C ($Ag_{6.25}P_{0.75}Si_{0.25}S_5I$) and 40 °C ($Ag_{6.75}P_{0.25}Si_{0.75}S_5I$), the EEC elements responsible for the electronic component of electrical conductivity (R_e, R_{dbe}/C_{dbe}) were not used for fitting. Thus, low-frequency linear/arc-shaped sections are fitted with EEC elements as lines/semicircles, while high-frequency sections – as high-frequency semicircles (Fig. 3).

According to Fig. 3, low-frequency linear sections/semicircles on Nyquist plots correspond to the capacitance of a double diffusion layer (C_{dl}) that arises at the crystal/electrode boundary, while the representation of the deformed high-frequency sections is associated with an ionic resistance (R_{ion}) with parallel capacitance (C_{ion}) of defect-limited regions. It should be noted that these defects are most likely small-angle boundaries, dislocations, *etc*. It is known [29] that during the growth of single crystals by directional solidification from a melt, the presence of these defects is observed quite often.

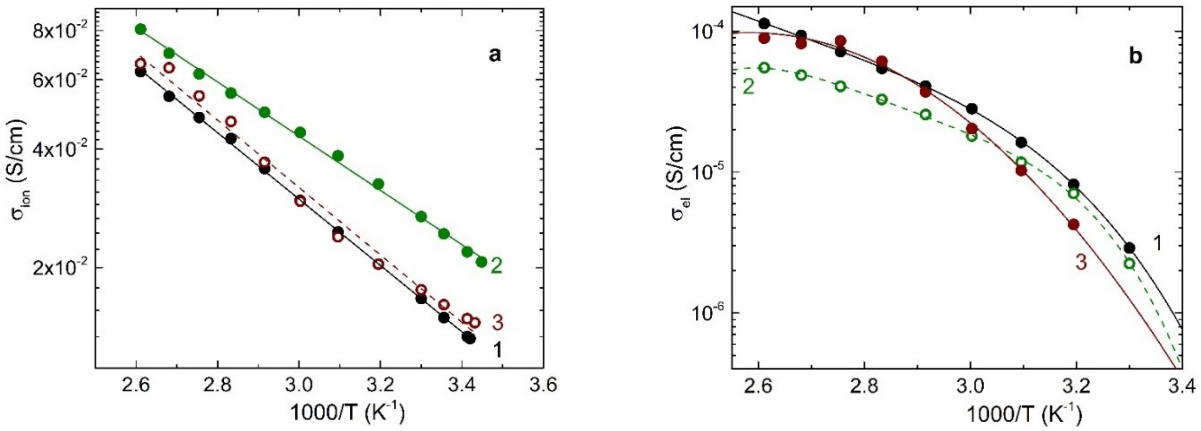

Fig. 4. Temperature dependences of ionic (a) and electronic (b) components of electrical conductivity for $Ag_{6.25}P_{0.75}Si_{0.25}S_5I$ (1), $Ag_{6.5}P_{0.5}Si_{0.5}S_5I$ (2) [21], and ($Ag_{6.75}P_{0.25}Si_{0.75}S_5I$ (3) single crystals.

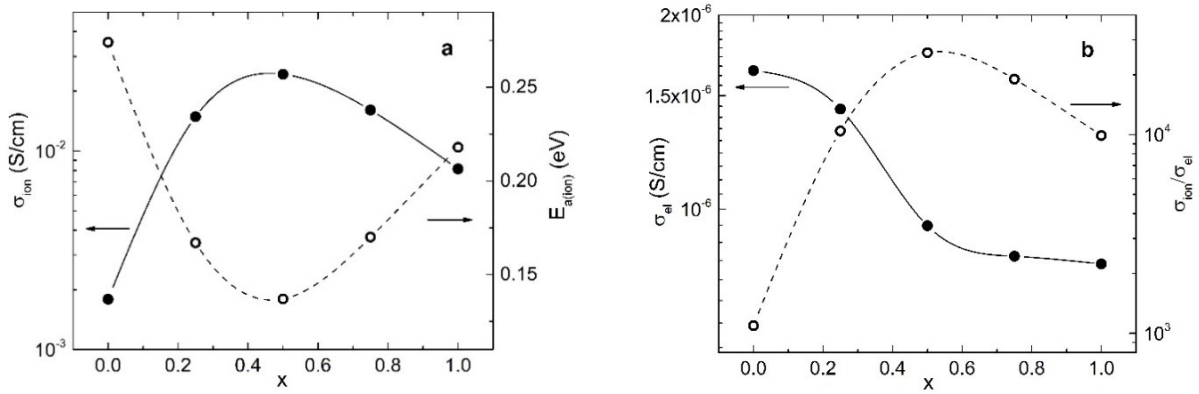

Fig. 5. Compositional dependences of the ionic component of electrical conductivity at 25 °C and its activation energy (a); compositional dependences of the electronic component of electrical conductivity estimated at 25 °C and the ratio between the ionic and electronic components of electrical conductivity (b).

In parallel with the elements (C_{dl}, R_{ion}/C_{ion}) associated with ion transport in EEC, elements responsible for the electronic component of electrical conductivity are included – volume electronic resistance R_e and electronic resistance R_{dbe} with parallel capacitance C_{dbe}, which arises at the boundaries between defects. It should be noted that these parameters affect the nature of Nyquist plots throughout the entire studied frequency range. Thus, the value of the ionic component of electrical conductivity can be calculated as $1/R_{ion}$, and the electronic component as $– 1/R_e + R_{dbe}$.

As a result of the analysis, the values of the ionic (in the entire studied temperature range) and electronic (within 30…110 °C ($Ag_{6.25}P_{0.75}Si_{0.25}S_5I$) and 40…110 °C ($Ag_{6.75}P_{0.25}Si_{0.75}S_5I$)) components of electrical conductivity were determined, and their temperature dependences were plotted in Arrhenius coordinates (Fig. 4).

It has been ascertained that the values of the ionic component of electrical conductivity (Fig. 4a) within the studied temperature range are linear for $Ag_{6.25}P_{0.75}Si_{0.25}S_5I$ and $Ag_{6.75}P_{0.25}Si_{0.75}S_5I$. In contrast, the electronic component of electrical conductivity (Fig. 4b) changes nonlinearly with increasing temperature. Regarding this, the activation energy can only be determined for the ionic component of electrical conductivity. It should be noted that similar temperature behavior of the components of electrical conductivity is also observed for the $Ag_{6.5}P_{0.5}Si_{0.5}S_5I$ single crystal [21].

Let us consider the effect of heterovalent cationic $P^{+5} \rightarrow Si^{+4}$ substitution on the change in the electrical parameters of $Ag_{6+x}(P_{1-x}Si_x)S_5I$ single crystals at room temperature (Fig. 5). It has been ascertained that the heterovalent cationic $P^{+5} \rightarrow Si^{+4}$ substitution leads to a monotonic nonlinear increase in ionic conductivity values (by one order of magnitude) and a corresponding decrease in its activation energy (Fig. 5a) compared to initial Ag_6PS_5I and Ag_7SiS_5I crystals. In contrast, the value of the electronic component of electrical conductivity estimated at 25 °C in the process of cationic $P^{+5} \rightarrow Si^{+4}$ substitution monotonically and nonlinearly decreases ($10^{-6} \rightarrow 10^{-7}$ S/cm) without the presence of extreme points (Fig. 5b). It is noteworthy that for all $Ag_{6+x}(P_{1-x}Si_x)S_5I$ single crystals, the ionic component of electrical conductivity exceeds the electronic component by 10^4 times, while for the initial quaternary chalcogenides, this parameter is 10^3 (Fig. 5b).

3.3. Ion transport mechanism

This work seeks to explain the increase in ionic conductivity and decrease in its activation energy in $Ag_{6+x}(P_{1-x}Si_x)S_5I$ solid solutions compared to the initial quaternary chalcogenides using peculiarities of their crystal structure (Fig. 2). As described above, the crystal structures of the studied solid solutions contain two symmetrically independent positions of silver for which SOF < 1. It should be noted that SOF(Ag2) < SOF(Ag1), which indicates greater delocalization in the crystal structures of silver in the Ag2 position compared to Ag1. Thus, the parameters of silver in the Ag2 position (SOF value, maximum distance d_{max} between positions (ion transport limiting), change in position coordination) will be more responsible for the efficiency of ion transport, and ion transport should be considered as ion diffusion through the "channels" formed by this position (Fig. 2). It has been ascertained that heterovalent cation $P^{+5} \rightarrow Si^{+4}$ substitu-tion leads to a decrease in SOF(Ag2) and the maximum distance (d_{max}) between these positions (Fig. 6). As a result, the values of these parameters for all solid solution compositions are less than for Ag_7SiS_5I, and in the case of $Ag_{6.25}P_{0.75}Si_{0.25}S_5I$ and $Ag_{6.5}P_{0.5}Si_{0.5}S_5I$ [21], less than for both initial chalcogenides (Fig. 6). This favorable change in ion transport conditions (Fig. 6) in solid solutions explains the general trend toward an increase in ionic conductivity and a decrease in its activation energy (Fig. 5a) compared to the initial Ag_6PS_5I and Ag_7SiS_5I, but does not explain why the ionic conductivity is higher for $Ag_{6.5}P_{0.5}Si_{0.5}S_5I$, and its activation energy is lower than for $Ag6_{.25}P_{0.75}Si_{0.25}S_5I$, although the considered structural descriptors should show the opposite.

An effort is made to consider the following equally important factor of ion transport efficiency, namely the change in coordination (displacement) of mobile positions relative to the centers of tetrahedra [AgS_3I] (Fig. 2). It is known [13, 18] that the greater this displacement (to the planes of triangles or edges), the lower the energy barrier required for ion transport.

For this purpose, [AgS_3] pyramids (Fig. 7) were constructed, which form the basis of [AgS_3I] tetrahedra (Fig. 2). The following parameters were calculated using Ag–S bond length values [21]: the distortion coefficient (D) and the effective coordination number (ECoN).

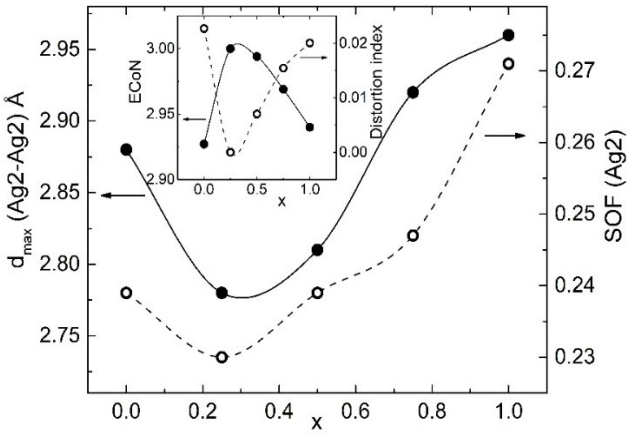

Fig. 6. Compositional dependences of the maximum distance between silver in the Ag2 position and SOF of Ag2. The inset shows the compositional dependences of the distortion coefficient and effective coordination number of [AgS_3] pyramids.

These parameters were used to measure the displacement of the chosen atom from its ideal, perfectly symmetrical geometry. Thus, D shows the variation in the distances between the central atom and its surrounding atoms, ECoN measures the "effective" contribution of each surrounding atom to the central atom bonding (depending on bond length) [27].

Thus, heterovalent $P^{+5} \rightarrow Si^{+4}$ substitution for all the studied solid solutions $Ag_{6+x}(P_{1-x}Si_x)S_5$ leads to a decrease in the degree of displacement of silver in the Ag2 position relative to the center of the triangular plane S1S2S1 compared to initial compunds, as indicated by the increase in ECoN values and the corresponding decrease in D (insert to Fig. 6). It is noteworthy that the smallest displacement of Ag2 (ECoN = 3; D = 0) relative to the plane of the triangle is observed precisely for the composition $Ag_{6.25}P_{0.75}Si_{0.25}S_5I$ (insert to Fig. 6), for which other structural parameters (SOF, d_{max}) are most optimal for efficient ion transport, while a further increase in silicon content leads to a gradual increase in the degree of displacement of the mobile position of Ag2 relative to the same plane, as indicated by a gradual increase in D and a decrease in ECoN (insert to Fig. 6).

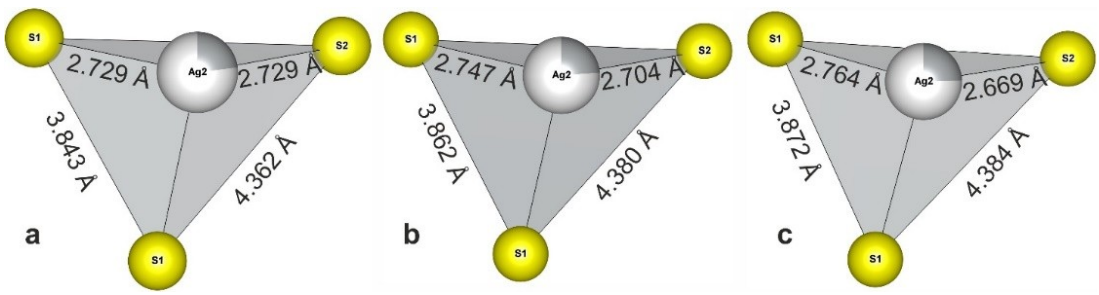

Fig. 7. [AgS_3] pyramids in crystal structures of $Ag_{6+x}(P_{1-x}Si_x)S_5I$ solid solutions: *1* – $Ag_{6.25}P_{0.75}Si_{0.25}S_5I$, *2* – $Ag_{6.5}P_{0.5}Si_{0.5}S_5I$, *3* – $Ag_{6.75}P_{0.25}Si_{0.75}S_5I$.

Thus, the relationship between structural parameters, which can increase or decrease ion transport efficiency (Fig. 6), manifests in the observed compositional dependences of ion conductivity and its activation energy.

4. Conclusions

In this work, $Ag_{6.25}P_{0.75}Si_{0.25}S_5I$ and $Ag_{6.75}P_{0.25}Si_{0.75}S_5I$ single crystals were obtained and studied. They were prepared by one-temperature synthesis followed by directional crystallization from the melt. X-ray structural analysis showed that both compositions crystallize in the argyrodite structure with the SG F-43m. It has been ascertained that heterovalent cation substitution $P^{+5} \rightarrow Si^{+4}$ occurs in one crystallographic position with the formation of common $[P(Si)S_4]$ tetrahedra, which are the basis of a rigid anion sublattice, while the cation sublattice of argentum is disordered.

Impedance spectroscopy showed that the studied materials are typical solid ionic conductors with the ionic component of electrical conductivity dominating the electronic component by four orders of magnitude. It was found that the ionic conductivity increases and its activation energy decreases with increasing the silicon content, while the electronic component monotonically decreases. The linear temperature dependence of ionic conductivity in Arrhenius coordinates allowed us to determine its activation parameters.

It has been shown that the increase in ionic conductivity is due to the following structural factors: a decrease in the site occupancy factor of mobile Ag2 positions, a reduction in the maximum distances between them, and a change in the local coordination of silver. The compromise found between different structural descriptors explains the non-monotonic compositional behavior of electrical conductivity and confirms the key role of crystal chemical factors in the formation of effective ion transport in argyrodite-like systems.

Acknowledgements

The authors also thank the Armed Forces of Ukraine for providing security to perform this work. This work has become possible only because of the resilience and courage of the Ukrainian Army.

References

1. Mitali J., Dhinakaran S., Mohamad A.A. Energy storage systems: a review. *Energy Storage Sav.* 2024. **1**. P. 166–216. https://doi.org/10.1016/j.enss.2022.07.002.
2. Nasajpour-Esfahani N., Garmestani H., Bagheritabar M. *et al.* Comprehensive review of lithium-ion battery materials and development challenges. *Renew. Sustain. Energy Rev.* 2024. **203**. P. 114783. https://doi.org/10.1016/j.rser.2024.114783.
3. Sung J., Heo J., Kim D.-H. *et al*. Recent advances in all-solid-state batteries for commercialization. *Mater. Chem. Front.* 2024. **8**. P. 1861–1887. https://doi.org/10.1039/D3QM01171B.
4. Jose S.A., Gallant A., Gomez P.L. *et al*. Solid-state lithium batteries: Advances, challenges, and future perspectives. *Batteries.* 2025. **11**. P. 90. https://doi.org/10.3390/batteries11030090.
5. Götz R., Streng R., Sterzinger J. *et al*. All-solid-state Li-ion batteries with commercially available electrolytes: A feasibility review. *InfoMat.* 2024. **6**. P. e12627. https://doi.org/10.1002/inf2.12627.
6. Wang H., Ozkan C.S., Zhu H., Li X. Advances in solid-state batteries: Materials, interfaces, characterizations, and devices. *MRS Bull*. 2023. **48**. P. 1221–1229. https://doi.org/10.1557/s43577-023-00649-7.
7. Wei R., Chen S., Gao T., Liu W. Challenges, fabrications and horizons of oxide solid electrolytes for solid-state lithium batteries. *Nano Select.* 2021. **2**. P. 2256. https://doi.org/10.1002/nano.202100110.
8. Lu J., Li Y. Perovskite-type Li-ion solid electrolytes: a review. *J. Mater. Sci: Mater. Electron.* 2021. **32**. P. 9736–9754. https://doi.org/10.1007/s10854-021-05699-8.
9. Yao P., Yu H., Ding Z. *et al*. Review on polymer-based composite electrolytes for lithium batteries. *Front Chem*. 2019. **7**. P. 522. https://doi.org/10.3389/fchem.2019.00522.
10. Ram Prasanth S., Prasannavenkadesan V., Katiyar V., Achalkumar A.S. Polymer electrolytes: evolution, challenges, and future directions for lithium-ion batteries. *RSC Appl. Polym*. 2025. **3**. P. 499–531. https://doi.org/10.1039/D4LP00325J.
11. Man B., Zeng Y., Liu Q. *et al*. A comprehensive review of sulfide solid-state electrolytes: Properties, synthesis, applications, and challenges. *Crystals*. 2025. **15**. P. 492. https://doi.org/10.3390/cryst15060492.
12. Kimura T., Nakano T., Sakuda A. *et al*. Crystal structure changes of thio-LISICON electrolytes in humid atmosphere. *J. Ceram. Soc. Jpn*. 2023. **131**. P. 166–171. https://doi.org/10.2109/jcersj2.23015.
13. Kawamura J. Ion conducting materials: superionic conductors and solid-state ionics, In: Brabazon D. (Ed.), *Encyclopedia of Materials: Composites*. 2017. P. 293–313. https://doi.org/10.1016/B978-0-12-803581-8.01724-0.
14. Hebb M.H. Electrical conductivity of silver sulfide. *J. Chem. Phys*. 1952. **20**. P. 185–190. https://doi.org/10.1063/1.1700165.
15. Wang T., Chen H.-Y., Qiu P.-F. *et al*. Thermo-electric properties of Ag_2S superionic conductor with intrinsically low lattice thermal conductivity. *Acta Phys. Sin*. 2019. **68**. P. 090201. https://doi.org/10.7498/aps.68.20190073.
16. Kuhs W.F., Nitsche R., Scheunemann K. The argy-rodites – a new family of tetrahedrally close-packed structures. *Mat. Res. Bull.* 1979. **14**. P. 241–248. https://doi.org/10.1016/0025-5408(79)90125-9.

17. Bindi L., Biagioni C. A crystallographic excursion in the extraordinary world of minerals: The case of Cu- and Ag-rich sulfosalts. *Acta Crystallogr. B.* 2018. **74**. P. 527–538. https://doi.org/10.1107/S2052520618014452.
18. Pogodin A.I., Studenyak I.P., Shender I.A. *et al*. Crystal structure, ion transport and optical properties of new high-conductivity $Ag_7(Si_{1-x}Ge_x)S_5I$ solid solutions. *J. Mater. Sci.* 2022. **57**. P. 6706–6722. https://doi.org/10.1007/s10853-022-07059-1.
19. Studenyak I.P., Pogodin A.I., Filep M.J. *et al*. Crystal structure and electrical properties of Ag_6PS_5I single crystal. *SPQEO.* 2021. **24**. P. 26–33. https://doi.org/10.15407/spqeo24.01.026.
20. Studenyak I.P., Pogodin A.I., Filep M.J. *et al*. Influence of heterovalent cationic substitution on electrical properties of $Ag_{6+x}(P_{1-x}Ge_x)S_5I$ solid solutions. *J. Alloys Compd.* 2021. **873**. P. 159784. https://doi.org/10.1016/j.jallcom.2021.159784.
21. Pogodin A., Shender I., Pop M. *et al*. Crystal growth and opto-electrical properties of $Ag_{6.5}P_{0.5}Si_{0.5}S_5I$ solid-state ionic conductor. *Mat. Res. Bull.* 2026. **195**. P. 113866. https://doi.org/10.1016/j.materresbull.2025.113866.
22. Studenyak I.P., Pogodin A.I., Studenyak V.I. *et al*. Electrical properties of copper- and silver-containing superionic $(Cu_{1-x}Ag_x)_7SiS_5I$ mixed crystals with argy-rodite structure. *Solid State Ionics*. 2020. **345**. P. 115183. https://doi.org/10.1016/j.ssi.2019.115183.
23. Rietveld H.M. A profile refinement method for nuclear and magnetic structures. *J. Appl. Crystallogr.* 1969. **2**. P. 65–71. https://doi.org/10.1107/S0021889869006558.
24. McCusker L.B., Von Dreele R.B. *et al*. Rietveld refinement guidelines. *J. Appl. Crystallogr.* 1999. **32**. P. 36–50. https://doi.org/10.1107/S0021889898009856.
25. Altomare A., Burla M.C., Camalli M. *et al*. EXPO: a program for full powder pattern decomposition and crystal structure solution. *J. Appl. Crystallogr.* 1999. **32**. P. 339–340. https://doi.org/10.1107/S0021889898007729.
26. Altomare A., Cuocci C., Giacovazzo C. *et al*. EXPO2013: a kit of tools for phasing crystal structures from powder data. *J. Appl. Crystallogr*. 2013. **46**. P. 1231–1235. https://doi.org/10.1107/S0021889813013113.
27. Momma K., Izumi F. VESTA 3 for three-dimensional visualization of crystal, volumetric and morphology data. *J. Appl. Crystallogr.* 2011. **44**. P. 1272–1276. https://doi.org/10.1107/S0021889811038970.
28. Huggins R.A. Simple method to determine electronic and ionic components of the conductivity in mixed conductors a review. *Ionics*. 2002. **8**. P. 300–313. https://doi.org/10.1007/BF02376083.
29. Rudolph P. Defect formation during crystal growth from the melt. In: Dhanaraj G., Byrappa K., Prasad V., Dudley M. (Eds.) *Springer Handbook of Crystal Growth*. Springer, 2010. P. 159–201. https://doi.org/10.1007/978-3-540-74761-1_6.

Authors and CV

Artem I. Pogodin, PhD, Associate Professor and Senior Researcher at the Uzhhorod National University. Authored over 100 scientific papers indexed in the Scopus database and 114 patents. The area of his scientific interests includes solid state chemistry, crystal growth and materials science. E-mail: artempogodin88@gmail.com, https://orcid.org/0000-0002-2430-3220

Mykhailo J. Filep, PhD, Associate Professor at the Ferenc Rákóczi II Transcarpathian Hungarian University. Authored over 100 scientific papers, 50 patents and 2 monographs. The area of his scientific interests includes solid state chemistry and materials science.
E-mail: mfilep23@gmail.com, http://orcid.org/0000-0001-7017-5437

Iryna O. Shender, lecturer and Senior Researcher at the Uzhhorod National University. Defended her PhD thesis at the Uzhhorod National University in 2024. Authored 45 scientific papers and 14 patents. The area of her scientific interests is electrical, optical and mechanical properties of superionic conductors. E-mail: shender95@gmail.com, https://orcid.org/0000-0003-1687-3634

Tetyana O. Malakhovska, PhD, Senior Researcher, and Head of the department of organization for the educational process for PhD students at the Uzhhorod National University. The author of 230 scientific publications, including 43 articles indexed in the Scopus database, 1 monograph and 22 patents of Ukraine. The area of her scientific interests includes solid state chemistry crystal growth, and materials science.
E-mail: t.malakhovska@gmail.com, https://orcid.org/0000-0001-7309-4894

Oleksandr P. Kokhan, PhD, Associate Professor at the Uzhhorod National University. Authored over 80 scientific papers indexed in the Scopus database and 95 patents of Ukraine. The area of his scientific interests includes inorganic chemistry, solid state chemistry, crystal growth, and materials science. E-mail: aleksandr.kokh@gmail.com, http://orcid.org/0000-0003-1534-6779

Vitalii Yu. Izai, PhD in Physics of Semiconductors and Dielectrics. Scientific Associate at the Faculty of Mathematics, Physics and Informatics, Comenius University Bratislava. Authored 40 articles and more than 20 patents. The area of his interests includes materials science, superionic materials for solid-state ionics, deposition and physical properties of thin films. E-mail: vitalii.izai@fmph.uniba.sk, https://orcid.org/0000-0001-7512-3388

Authors' contributions

Pogodin A.I.: writing – original draft, methodology, writing – review & editing.
Filep M.J.: investigation, writing – original draft.
Shender I.O.: supervision, conceptualization, investigation, writing – original draft.
Malakhovska T.O.: methodology, writing – review & editing.
Kokhan O.P.: visualization, conceptualization.
Izai V.: methodology, investigation.

Взаємозв'язок між структурою та властивостями у твердих розчинах $Ag_{6+x}(P_{1-x}Si_x)S_5I$ зі структурою аргіродиту

А.І. Погодін, М.Й. Філеп, І.О. Шендер, Т.О. Малаховська, О.П. Кохан, В. Ізай

Анотація. У даній роботі одержано та досліджено монокристали твердих розчинів $Ag_{6.25}P_{0.75}Si_{0.25}S_5I$ та $Ag_{6.75}P_{0.25}Si_{0.75}S_5I$. Синтез монокристалів здійснено однотемпературним методом, а їх вирощування проводилось методом спрямованої кристалізації з розплаву. Вирощено монокристали діаметром близько 1.2 см та довжиною 3–4 см. Кристалічну структуру вирощених монокристалів досліджено методом РФА з використанням повнопрофільного аналізу Рітвельда. Встановлено, що тверді розчини кристалізуються у просторовій групі F-43m, $Z = 4$ з параметрами $a = 10.549$ Å ($Ag_{6.25}P_{0.75}Si_{0.25}S_5I$) та $a = 10.604$ Å ($Ag_{6.75}P_{0.25}Si_{0.75}S_5I$). Електричні властивості досліджено методом імпедансної спектроскопії у широкому температурному та частотному діапазонах. Показано, що електропровідність має переважно іонний характер, причому іонна складова у 10^4 разів перевищує електронну. Виявлено, що зі збільшенням вмісту кремнію іонна електропровідність зростає (до 10^{-2} См/см), а її енергія активації зменшується. Отримані результати пояснено особливостями кристалічної структури, зокрема змінами позиції, координації та просторового розташування рухливих іонів Ag^+.

Ключові слова: аргіродити, монокристали, іонна провідність, тверді розчини.